Outstanding Photocurrent Density and Incident Photon-to-Current Conversion Efficiency of Liquid-State NiO Perovskite-Sensitized Solar Cells

Hussain Alessa,* Mohamad Firdaus Mohamad Noh, Inzamam Nawas Nawas Mumthas, Kahagala Gamage Upul Wijayantha, and Mohd Asri Mat Teridi*

Abstract

The efficiency and photocurrent density reported for p-type-sensitized solar cells up to now are still lagging behind that of the n-type counterparts, limiting the successful development of p–n tandem cells. To circumvent this issue, NiO thin film is fabricated by the aerosol-assisted chemical vapor deposition (AACVD) technique and used in p-type solar cells. A systematic study is conducted to comprehend the correlation between NiO thickness and the power conversion efficiency (PCE) of liquid-state NiO-based sensitized solar cells. By carefully designing the cell components, this type of device demonstrates the highest photocurrent density (J_{sc}) exceeding 18 mA cm_2 when using iodine/triiodide as the redox shuttle matching the one produced by the TiO_2 counterpart. This is accomplished by 1) using the AACVD technique for the one-step deposition of compact and mesoporous NiO electrodes, 2) optimizing the thickness of the NiO layer through controlling the deposition time, and 3) adopting methylammonium lead iodide ($CH_3NH_3PbI_3$) as a light harvester prepared via a sequential deposition method.

Introduction

Solar energy is proposed as the best candidate among other renewable energy sources as it is a clean, abundant, and an everlasting energy source. However, its establishment requires the capability of delivering a high light-to-electricity efficiency at a reasonable cost.[1] Among the solar cell types, dye-sensitized solar cells (DSSCs) was demonstrated to meet the aforementioned requirement. Since the proposed concept of liquid-state tandem solar cells (LS TSCs),[2] tremendous amount of work has focused on the adjustment of both compartments: photoanode and photocathode. As for meeting the requirement of this concept, the photocurrent density (J_{sc}) of both the photoanode and photocathode should be matched. With the sensitized TiO_2 being able to deliver up to 18 mA cm_2,[3] the highest reported J_{sc} for sensitized NiO is still far behind. This has hindered the complete achievement of the tandem concept so far. It is well known that each component of a DSSC contributes to the overall conversion efficiency. Thus, several approaches have been followed for improving the properties of these components: semiconductors, sensitizers, and the utilized redox couple electrolyte, aiming to improve the efficiency parameters of LS p-type DSSCs and eventually meet the requirement for constructing LS p–n TSCs. To date, NiO has shown great potential as a photocathode and the corresponding p-type DSSC has reached an efficiency of up to 2.51% upon using $[Fe(acac)_3]_{0/1}$_ as the new redox mediator.[4] Yet, the NiO photocathode still needs further improvement to be able to produce the same photocurrent as the photoanode counterpart. The efficacy of NiO can be further enhanced by introducing dopants, passivating the surface of the photocathode, developing nanocomposites, and modifying nanostructures [5–8].

From the viewpoint of sensitizers, a series of organic dyes was adopted in LS p-type DSSCs but the poor absorption coefficient of the dyes hampers the efficient light-harvesting ability of the device.[3] Therefore, organometallic halide perovskites, based on $CH_3NH_3PbI_3$ and its derivatives, which possess superior optical and electrical properties, have been investigated as a replacement for the conventional dye sensitizer. These types of light absorbers have a relatively high absorption coefficient with tunable low bandgaps which enable them to harvest the incident light effectively to the near-infrared (IR) region.[9–11] Although state-of-the-art solid-state perovskite solar cells have exhibited impressive efficiency and improved stability,[12] the development of the liquid state device based on perovskite sensitizers still has research significance, particularly for tandem and semitransparent solar cells.

Therefore, in this work, we develop LS p-type solar cells using the NiO(photocathode)/$CH_3NH_3PbI_3$(sensitiser) system, and we demonstrate the following: 1) the introduction of NiO films fabricated by the aerosol-assisted chemical vapor deposition (AACVD) to the solar cell community, 2) an exceptionally high J_{sc} of over 18 mA cm_2 for LS p-type-sensitized-NiO solar cells, 3) a remarkable PCE for LS $CH_3NH_3PbI_3$-sensitized NiO solar cells using $I_/I_3$_ as the redox couple, and 4) an outstanding incident photon-to-current conversion efficiency (IPCE) reported for LS-NiO solar cells. To the best of our knowledge, there is only one article that has demonstrated the fabrication of liquid-state NiO perovskite-sensitized solar cells with the best reported J_{sc} and PCE, using the traditional $I_/I_3$_ redox shuttle, of 9.47 mA cm_2 and 0.71%, respectively.[13] Our present work signifies the potential of AACVD for the deposition of NiO photocathode toward boosting the efficiency of p-type solar cells.

2. Results and Discussion

Typically, the fabrication of electron/hole transport layers requires two steps, i.e., depositing a compact layer followed by a mesoporous layer. Contrary to the methods reported in the literature, we fabricated NiO from a single precursor source in one-step deposition using the AACVD method, reducing the time for making such a photoelectrode. The utilization of AACVD as a mean for making nanostructured thin films has some advantages over various deposition methods, such as good adhesion of the deposited films on the substrates and the onestep process. The NiO photocathode was then sensitized with $CH_3NH_3PbI_3$ via sequential deposition. Herein, sequential deposition was adopted for sensitizing the NiO electrodes due to the fact that this method outperforms the unmodified one-step spin coating of $CH_3NH_3PbI_3$. The adaptation of sequential deposition would lead to better $CH_3NH_3PbI_3$ surface coverage on NiO electrodes, thus improving the sensitisation of NiO electrodes, resulting in a higher degree of light absorption, in other words, a high J_{sc} and PCE. Figure 1 shows a schematic diagram of the electronic structure and charge transfer mechanism of the fabricated device. During light illumination, $CH_3NH_3PbI_3$ absorbs the incident photons, leading to the formation of excitons that then can be separated by injecting holes to the valence band of NiO, whereas electrons are injected to the electrolyte. The open-circuit voltage (V_{oc}) is defined as the difference between the redox couple potential and the valence band of NiO.

NiO electrodes sensitized with $CH_3NH_3PbI_3$ were characterized by X-ray diffaction (XRD) to evaluate the purity of the deposited films. It is evident from Figure 2a that all diffraction peaks belonging to NiO can be indexed to the rhombohedral NiO structure (JCPDS-ICDD (PDF# 01-089-3080)).[14] XRD peaks labeled with (hkl) planes correspond to the tetragonal perovskite phase of $CH_3NH_3PbI_3$, suggesting the successful deposition of the light absorber on NiO photocathode. Figure 2(b,c) shows the scanning electron microscopy (SEM) images of the NiO electrodes sensitized with $CH_3NH_3PbI_3$ using a two-step approach. A cross-sectional view of a FTO/NiO/$CH_3NH_3PbI_3$ sample is also presented. It is shown that compact and mesoporous NiO layers are formed. This may be due to the annealing period during deposition time. While increasing the NiO thickness by increasing the deposition time, the underlayers are crushed to form a compact layer.

Figure 3a shows the absorption trends of NiO deposited for 30, 45, 60, and 75 min as well as the respective absorption spectra after being sensitized with the perovskite. Both bare NiO and perovskite-sensitized NiO films demonstrate higher light absorption upon increasing the deposition time of the NiO photocathode layer. This could be ascribed to 1) the thicker NiO film which corresponds to an improved mesoporous structure, leading to a greater light scattering effect,[15] and 2) the larger surface area of the labyrinthine NiO network that enhances the loading of $CH_3NH_3PbI_3$ on the NiO electrodes.[16] We evaluated the effect of changing the NiO deposition time on the solar cells' performance by carrying out current–voltage (I–V) measurements at 1000Wm_2 AM 1.5G simulated sunlight and the related IPCE measurement. I–V measurement was carried out as soon as the electrolyte was loaded into the cells to minimize the performance loss of the devices due to the solubility of perovskite in the electrolyte. As shown in Figure 3b, a significant increment of J_{sc} value is observed as the NiO deposition time is increased to 60 min because the greater light absorption of the thicker NiO layer promotes the number of electron–hole pairs generated. In addition, the IPCE measurement (Figure 3c) confirms strong absorption, starting from _340 nm, around the bandgap of NiO, sweeping the ultraviolet region and the visible region reaching the maximum at 760 nm, where the decrease occurs around the bandgap of $CH_3NH_3PbI_3$.

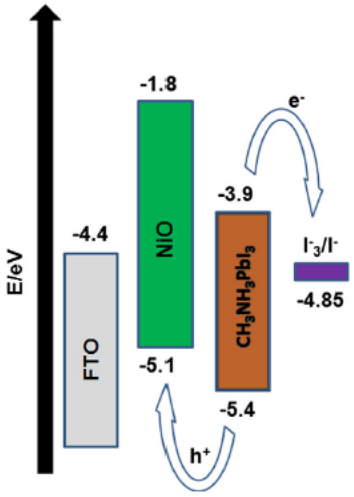

Figure 1. Schematic diagram of the energy levels of the components and charge transfer process in liquid-state $CH_3NH_3PbI_3$-sensitized NiO solar cells.

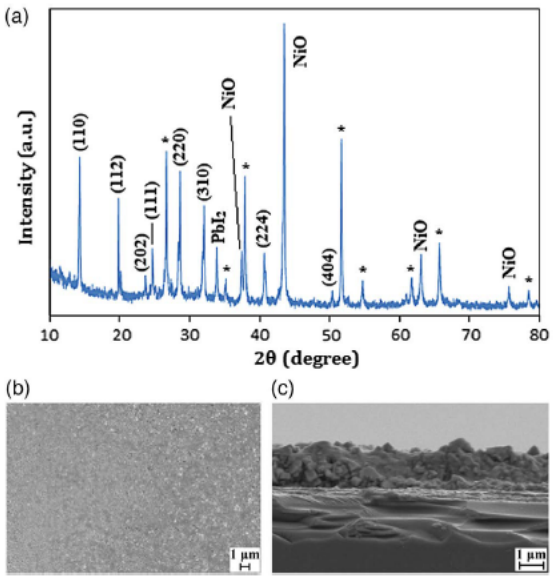

Figure 2. a) The XRD of FTO/NiO/$CH_3NH_3PbI_3$ (peaks marked with [*hkl*] and asterisk symbol represents perovskite and FTO, respectively). b) Top-view SEM image of the NiO thin film after being sensitized with $CH_3NH_3PbI_3$. c) Cross-sectional SEM image of the structure FTO/NiO/$CH_3NH_3PbI_3$.

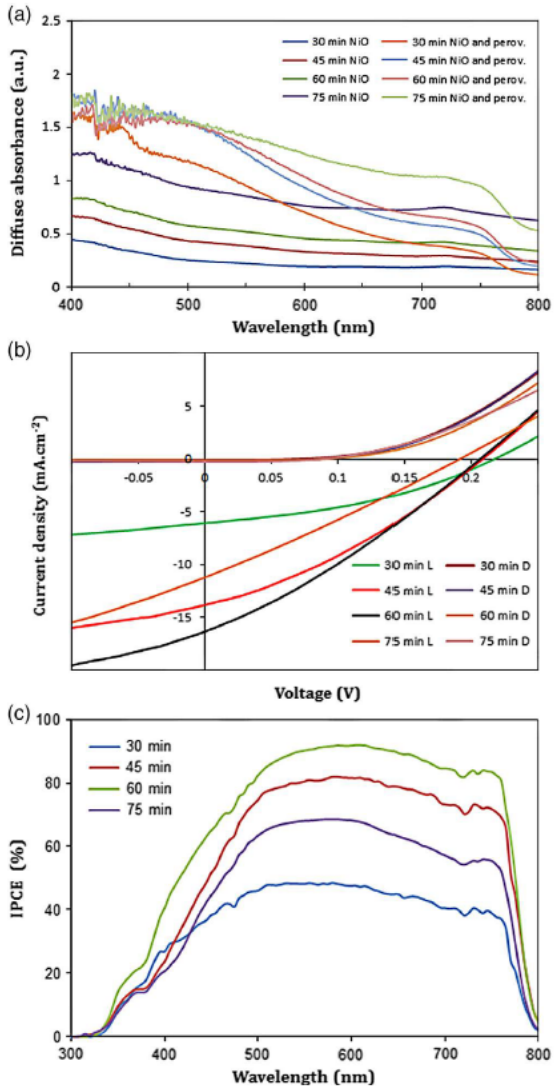

Figure 3. a) UV–vis absorption spectra of NiO electrodes prepared at different deposition times by AACVD, before and after being sensitized with $CH_3NH_3PbI_3$, and b) current density—voltage (J–V) curves respond to 1 sun illumination for various LS NiO perovskite-sensitized solar cells. Each curve is labelled with the deposition time of NiO and its behavior in the dark (D) or during light illumination (L). c) The IPCE spectra of the respective devices.

The trends in Figure 4 show the correlation between the photovoltaic parameters and NiO deposition time. It is noted that the efficiency of the device is primarily governed by J_{sc}. In general, the limit of NiO deposition time is 60 min, at which the PCE and J_{sc} reach the optimum values. As described earlier, the greater thickness of the NiO film elevates the light absorption ability of the perovskite-sensitized photocathode and positively impacts the photogeneration of charges. Nevertheless, the performance of the solar cell experiences a drop by further increasing the deposition time to 75 min which could be attributed to the high series resistance and low shunt resistance. This stems from the larger distance charge has to travel through the NiO film before being collected on the external circuit. Such a condition intensifies the charge recombination rate within the device.[17] The J_{sc} obtained from the current–voltage curves are confirmed and supported by the IPCE measurement, and the calculated short-circuit current densities are 9.47, 15.69, 18.08, and 12.81 mA cm_2 for devices using NiO deposited for 30, 45, 60, and 75 min. The obtained J_{SC} values in this work are higher than the one reported by Wang et al.[13] due to the improvement in the engineering of the interfaces of the device. Herein, it is worth mentioning that the perovskite sensitizer is rapidly soluble in the electrolyte within 10 min of operating time under light illumination, a phenomenon which is similar to the previous report.[18] Therefore, the stability of the devices requires further improvement. This could be done by introducing additives or using other suitable redox mediators which will be discussed in a separate report.

3. Conclusions

In summary, we demonstrated the successful introduction of NiO made by AACVD to the p-type solar cells field. We showed the effect of the NiO film thickness on the performance of liquid state perovskite-sensitized solar cells. By carefully optimizing the cell conditions, we obtained the highest J_{SC} and a very impressive PCE for these types of cells. We believe that this work would put us a step ahead in solving the problem of producing J_{sc} for p-type, side matching the n-type counterpart. The discovery in this work would definitely assist in advancing the renewable energy community toward fabricating liquid-state tandem solar cells.

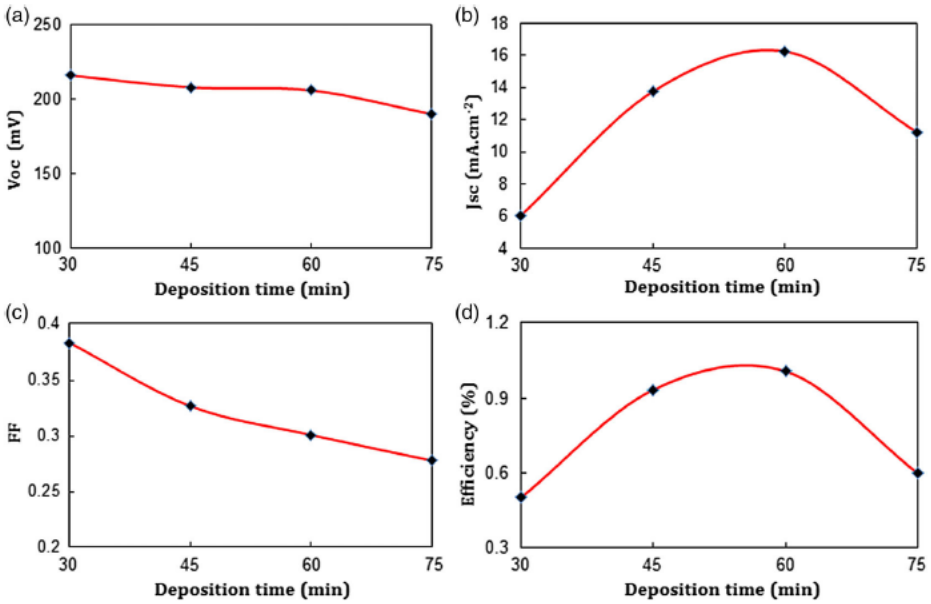

Figure 4. The correlation between the NiO deposition time and the photovoltaic parameters.

4. Experimental Section

Device Fabrication: SnO_2:F substrates (Pilkington group limited, TEC C15) were cut to a rectangular shape with 1 _ 2 cm_2 (2 cm_2) size and cleaned successively in soapy water, deionized water, 2-propanol, acetone, and ethanol, each of which is done in an ultrasonic bath for 15 min. Then, the substrates were kept in ethanol prior to using the cells in the fabrication process. Samples were etched using Zn powder and 2 M $HCl_{(aq)}$ to define the area and reduce the leakage current. NiO was then deposited on FTO substrates by means of the AACVD method from a single precursor solution (0.05 M Nickel (II) actylacetonate; $Ni(acac)_2$ 95% supplied by Aldrich, 2-dimethylaminoethanol (DMAE)≥ 98.0% provided by Fluka). Initially, 50mM $Ni(acac)_2$ was dissolved in toluene, and 1.5 mL DMAE was added drop wise while stirring the solution at 50 _C to enhance the solubility of the Ni complex and the volatility. A fixed area of the substrates was masked with microscope glass (to allow for making contact with the wires later), and AACVD was used for depositing NiO on the substrates. A fixed amount of the NiO precursor was placed in a two-neck round-bottomed flask and positioned above the piezoelectric modulator of an ultrasonic humidifier. Upon switching on the humidifier, the aerosol was generated and guided by carrier gas, air at a flow rate of 175.18 mL min_{-1}, to a three-neck round-bottomed flask where larger particles were trapped. The rest of the aerosol was diluted by more air entering the second flask, at a fixed flow rate (2340 mL min_{-1}), which then continued the transportation to the deposition chamber where it deposited on the substrates placed on a hotplate. The hotplate temperature was set to 475 _C, and the deposition time was varied to 30, 45, 60, and 75min. The mechanism of forming NiO thin layers on the substrates was denoted by the chemical equations as follows

$$Ni(acac)_{2(s)} + toluene_{(l)} + 2\text{-}DMAE_{(l)} \rightarrow Ni(acac)_{2(l)} \quad (1)$$

$$Ni(acac)_{2(l)} + air_{(g)} \rightarrow NiO_{(s)} + byproducts \quad (2)$$

Then FTO/NiO electrodes were coated with $CH_3NH_3PbI_3$ using the sequential deposition method. This involved preparing two solutions in separate sample tubes, 1 M PbI_2 in anhydrous DMF and 62.5mM CH_3NH_3I in dry isopropanol. About 50 µL PbI_2 was cast on FTO/NiO and spun at 2000 rpm for 10 s twice before drying at 70 _C for 20 min. This was followed by immersing FTO/NiO/PbI_2 in the CH_3NH_3I solution for 60 s, dried at laboratory temperature for 1 min, and annealed at 70 _C for 10 min. The FTO/NiO/$CH_3NH_3PbI_3$ electrodes were filled with the I_-/I_{3-} electrolyte (500mM LiI, 250mM I_2, 30mM $CO(NH_2)_2$, and 300mM tert-butylpyridine in anhydrous ethyl acetate) and sandwiched with Pt as a counter electrode.

Toolbox Techniques: The phase formation and the crystallinity of NiO electrodes were evaluated by a Bruker D8 X-ray diffractometer, operating with high-density Cu Kα (λ ¼ 0.154 nm) radiation using a PSD detector at a scan rate of 0.008o s_{-1}, and the scanned angles were 10_–80_. The surface morphology and the thickness of the films were studied using a Leo 1530 VP field-emission gun SEM (Joel, Hertfordshire, UK) at an accelerating voltage of 5 kV and a working distance of 5.9 mm. The spectroscopic measurements were carried out using a dual beam Perkin-Elmer Lambda 35 UV–vis spectrometer (Cambridge, UK) with a RSA-PE-20

labsphere accessory. The current–voltage measurements were evaluated using a potentiostat/galvanostat (Eco Chemie micro-AutoLab type III or Eco Chemie AutoLab PGSTAT-12), linked by a computer and light source, giving light intensity of 10_3mWcm$_{-2}$. AM 1.5G simulated light was used as the illumination light source. The calculated photocurrent at the short-circuit conditions was obtained by the IPCE, using a 75W Xenon lamp connected to a monochromator (Bentham, TMc300), and the IPCE system was calibrated by a UV-enhanced silicon photodiode (Bentham).

Acknowledgements

H.A. would like to thank the Saudi Cultural Bureau (SACB) in London for the financial support. M.A.M.T. and M.F.M.N. would like to thank Universiti Kebangsaan Malaysia for the financial supports through Dana Impak Perdana (DIP-2018-009).

References

[1] N. A. Ludin, N. I. Mustafa, M. M. Hanafiah, M. A. Ibrahim, M. Asri Mat Teridi, S. Sepeai, A. Zaharim, K. Sopian, Renew. Sustain. Energy Rev. 2018, 96, 11.
[2] J. He, H. Lindström, A. Hagfeldt, S.-E. Lindquist, Sol. Energy Mater. Sol. Cells 2000, 62, 265.
[3] S. Mathew, A. Yella, P. Gao, R. Humphry-Baker, B. F. E. Curchod, N. Ashari-Astani, I. Tavernelli, U. Rothlisberger, M. K. Nazeeruddin, M. Grätzel, Nat. Chem. 2014, 6, 242.
[4] I. R. Perera, T. Daeneke, S. Makuta, Z. Yu, Y. Tachibana, A. Mishra, P. Bäuerle, C. A. Ohlin, U. Bach, L. Spiccia, Angew. Chemie Int. Ed. 2015, 54, 3758.
[5] L. Wei, L. Jiang, S. Yuan, X. Ren, Y. Zhao, Z. Wang, M. Zhang, L. Shi, D. Li, Electrochim. Acta 2016, 188, 309.
[6] L. Favereau, Y. Pellegrin, L. Hirsch, A. Renaud, A. Planchat, E. Blart, G. Louarn, L. Cario, S. Jobic, M. Boujtita, F. Odobel, Adv. Energy Mater. 2017, 7, 1601776.
[7] R. Tan, Z. Wei, J. Liang, Z. Lv, B. Chen, J. Qu, W. Yan, J. Ma, Mater. Res. Bull. 2019, 116, 131.
[8] R. Brisse, R. Faddoul, T. Bourgeteau, D. Tondelier, J. Leroy, S. Campidelli, T. Berthelot, B. Geffroy, B. Jousselme, ACS Appl. Mater. Interfaces 2017, 9, 2369.
[9] A. Kojima, K. Teshima, Y. Shirai, T. Miyasaka, J. Am. Chem. Soc. 2009, 131, 6050.
[10] M. M. Lee, J. Teuscher, T. Miyasaka, T. N. Murakami, H. J. Snaith, Science 2012, 338, 643.
[11] O. Malinkiewicz, A. Yella, Y. H. Lee, G. M. Espallargas, M. Graetzel, M. K. Nazeeruddin, H. J. Bolink, Nat. Photonics 2014, 8, 128.
[12] A. R. Bin Mohd Yusoff, P. Gao, M. K. Nazeeruddin, Coord. Chem. Rev. 2018, 373, 258.
[13] H. Wang, X. Zeng, Z. Huang, W. Zhang, X. Qiao, B. Hu, X. Zou, M. Wang, Y.-B. Cheng, W. Chen, ACS Appl. Mater. Interfaces 2014, 6, 12609.
[14] M. A. Mat-Teridi, A. A. Tahir, S. Senthilarasu, K. G. U. Wijayantha, M. Y. Sulaiman, N. Ahmad-Ludin, M. A. Ibrahim, K. Sopian, Phys. Status Solidi RRL. 2014, 8, 982.
[15] N. A. Arzaee, M. F. Mohamad Noh, A. Ab Halim,
M. A. F. Abdul Rahim, N. A. Mohamed, J. Safaei, A. Aadenan, S. N. Syed Nasir, A. F. Ismail, M. A. Mat Teridi, Ceram. Int. 2019, 45, 16797.
[16] M. F. Mohamad Noh, C. H. Teh, R. Daik, E. L. Lim, C. C. Yap, M. A. Ibrahim, N. Ahmad Ludin, A. R. bin Mohd Yusoff, J. Jang, M. A. Mat Teridi, J. Mater. Chem. C 2018, 6, 682.
[17] M. F. Mohamad Noh, M. F. Soh, M. A. Riza, J. Safaei, S. N. F. Mohd Nasir, N. W. Mohamad Sapian, C. H. Teh, M. A. Ibrahim, N. Ahmad Ludin, M. A. Mat Teridi, Phys. Status Solidi 2018, 255, 1700570.
[18] J. H. Im, C. R. Lee, J. W. Lee, S. W. Park, N. G. Park, Nanoscale 2011, 3, 4088.